HOKKAIDO UNIVERSITY

Title	A step-by-step simulation code for estimating yields of water radiolysis species based on electron track-structure mode in the PHITS code
Author(s)	Matsuya, Yusuke; Yoshii, Yuji; Kusumoto, Tamon et al.
Citation	Physics in medicine and biology, 69, 035005 https://doi.org/10.1088/1361-6560/ad199b
Issue Date	2024-01-19
Doc URL	https://hdl.handle.net/2115/93935
Rights	This is the Accepted Manuscript version of an article accepted for publication in Physics in Medicine & Biology. IOP Publishing Ltd is not responsible for any errors or omissions in this version of the manuscript or any version derived from it. The Version of Record is available online at https://doi.org/10.1088/1361-6560/ad199b
Type	journal article
File Information	Matsuya2024.pdf

Hokkaido University Collection of Scholarly and Academic Papers : HUSCAP

A step-by-step simulation code for estimating yields of water radiolysis species based on electron track-structure mode in the PHITS code

Yusuke Matsuya[1,2*†], Yuji Yoshii[3†], Tamon Kusumoto[4], Ken Akamatsu[5], Yuho Hirata[1], Tatsuhiko Sato[1], Takeshi Kai[1]

[1] Nuclear Science and Engineering Center, Research Group for Radiation Transport Analysis, Japan Atomic Energy Agency (JAEA), 2-4 Shirakata, Tokai, Ibaraki, 319-1195, Japan
[2] Faculty of Health Sciences, Hokkaido University, Kita-12 Nishi-5, Kita-ku, Sapporo, Hokkaido, 060-0812, Japan
[3] Department of Radiological Technology, Faculty of Health Sciences, Hokkaido University of Science, Maeda 7-15, Teine-ku, Sapporo 006-8585, Japan
[4] National Institutes for Quantum Science and Technology, 4-9-1 Anagawa, Inage-ku, 263-8555 Chiba, Japan
[5] Institute for Quantum life Science, Quantum Life and Medical Science Directorate, National Institutes of Quantum and Radiological Science and Technology (QST), 8-1-7 Umemidai, Kizugawa-shi, Kyoto, 619-0215, Japan

[*] Corresponding author: matsuya.yusuke@hs.hokudai.jp (Yusuke Matsuya)
[†] These authors contributed equally

ABSTRACT

Objective. Time-dependent yields of chemical products resulting from water radiolysis play a great role in evaluating DNA damage response after exposure to ionizing radiation. Particle and Heavy Ion Transport code System (PHITS) is a general-purpose Monte Carlo simulation code for radiation transport, which simulates atomic interactions originating from discrete energy levels of ionizations and electronic excitations as well as molecular excitations as physical stages. However, no chemical code for simulating water radiolysis products exists in the PHITS package. *Approach.* Here, we developed a chemical simulation code dedicated to the PHITS code, hereafter called *PHITS-Chem* code, which enables the calculation of the G values of water radiolysis species ($^{\bullet}OH$, e_{aq}^{-}, H_2, H_2O_2 etc.) by electron beams. *Main results.* The estimated G values during 1 μs are in agreement with the experimental ones and other simulations. This *PHITS-Chem* code also simulates the radiolysis in the presence of OH radical scavengers, such as tris(hydroxymethyl)aminomethane and dimethyl sulfoxide. Thank to this feature, the contributions of direct and indirect effects on DNA damage induction under various scavenging capacities can be analyzed. *Significance.* This chemical code coupled with PHITS could contribute to elucidating the mechanism of radiation effects by connecting physical, physicochemical, and chemical processes.

Key words: electrons, Monte Carlo simulation, PHITS code, water radiolysis, DNA damage

1. INTRODUCTION

When the human body is exposed to ionizing radiation, biological effects such as apoptosis, mutation and carcinogenesis are occasionally induced (Joiner *et al* 2009). Such radiation effects are predominantly attributable to DNA damage induction by physical interaction with radiation and chemical reactions of water radiolysis species with the DNA in cells, which are called direct and indirect effects (Hall & Giaccia 2006). Amongst these, indirect effects within cells can induce more DNA lesions compared to direct effects under low linear energy transfer (LET) irradiation (Lampe *et al* 2018), which is mainly attributed to OH radicals (Peak *et al* 1995, Tomita *et al* 1998). To precisely understand the mechanisms underlying the biological effects by ionizing radiation, it is essential to mechanistically evaluate the time-dependent yields (generally noted as G values, that is, the chemical products yield per 100 eV) of chemical products generated by water radiolysis.

To evaluate the yield of the chemical species, the spatial distribution of each atomic interaction along radiation track is essential (Kai *et al* 2023). There are several Monte Carlo simulation codes for physical processes, such as PARTRAC (Friedland *et al* 2011), Kyushu University Radiobiology Unit Code (KURBUC) (Uehara 1986), Geant4-DNA (Incerti 2010), RITRACK (Plante & Cucinotta 2008), TRACEL (Tomita *et al* 1997), WLTrack (Date *et al* 2007), and Particle and Heavy Ion Transport code System (PHITS) (Sato *et al* 2018). They allow the simulation of atomic interactions, such as ionization, electronic excitation, and dissociative electron attachment (DEA) (Boudaıffa *et al* 2000). Chemical simulation codes have been also developed in conjunction with physical codes, such as PARTRAC (Kreipl *et al* 2009), KURBUC (Uehara & Nikjoo 2006), TRACEL (Tomita *et al* 1997), and Geant4-DNA (Shin *et al* 2019, 2021), however, the initial yields of chemical products (particularly hydrated electron e_{aq}^-) estimated by the most of codes are adjusted to reproduce yields using models of ionizations, excitations, geminate recombination ($e^- + H_2O^+ \rightarrow H_2O^*$, so called electron-hole recombination), and relaxation (Tomita *et al* 1997, Uehara & Nikjoo 2006, Kreipl *et al* 2009, Shin *et al* 2019, 2021). Amongst the physical simulation codes, PHITS is a general-purpose code for radiation transport, in which electron track structure until down to 1 meV can be simulated in liquid water (Kai *et al* 2015a, 2015b). This modality is known as the *PHITS-ETS* mode (Matsuya *et al* 2019). Therefore, the *PHITS-ETS* mode is expected to precisely provide the initial yield of e^- in the physical stages (Kai *et al* 2023). However, a chemical code for simulating products of water radiolysis does not exist in the PHITS code.

We developed a chemical code dedicated to PHITS (*PHITS-Chem* code), that allows calculating G values of various types of chemical products ($^{\bullet}OH$, e_{aq}^-, H_2, H_2O_2 etc) as a function of time after irradiation using a step-by-step (SBS) method (Plante 2021). We validated the *PHITS-Chem* code by comparing the simulated G values in a wide time scale, ranging from 1 ps to 1 μs with the experimental values and other simulations. One of the advantages of the *PHITS-Chem* code is its ability to handle OH radical scavengers, such as Tris (hydroxymethyl)aminomethane (Tris) and dimethyl sulfoxide (DMSO), and it is useful for analyzing the initial yields of DNA damage for various scavenging capacities. We present the characteristics of the *PHITS-Chem* code, which can contribute to precisely understanding induction mechanisms of DNA damage.

2. METHOD

The electron track-structure mode *PHITS-ETS* (Matsuya *et al* 2019) was used to obtain the spatial distribution of each atomic interaction along the electron track. In this study, we developed the *PHITS-Chem* code that includes models of physicochemical and chemical stages. It should be noted that the formation of hydrated electron and the electron-hole recombination have been already considered in the physical stage simulation of *PHITS-ETS* mode (Matsuya *et al* 2019, Kai *et al* 2023). Figure 1 summarizes the simulation flow of the physical and chemical stages of the PHITS code. This chemical code will be included in the PHITS package in the near future. As shown in Fig. 1, PHITS track-structure simulation has to be performed first to output coordinates and types of atomic interactions (physical stage), and then chemical stage simulation can be performed by reading the output data into external chemical code. N_p is the number of radiation particles and T_E is the tracking end time in the chemical simulation. The time-dependent G values can be graphically obtained using the ANGEL software included in the PHITS package (see Fig. S1 in the *Supplementary file*). In this study, the benchmark tests of comparing experimental time-dependent G values and the energy-dependence on primary yield (G value at 1 μs) calculated by other codes with those results calculated by the developed chemical code were performed. The developed code was also applied to DNA damage analysis for indirect effects. The setup of the *PHITS-ETS* mode (physical stage) and details of *PHITS-Chem* code (physicochemical and chemical stages) are described as below.

2.1. Physical stage

The *PHITS-ETS* mode must be activated in certain regions in the PHITS simulation world. In the *PHITS-ETS* mode, ionization ($1b_1$, $3a_1$, $1b_2$, $2a_1$, and $1a_1$), electronic excitations (A^1B_1, B^1A_1, Rydberg, and collective), DEA, intramolecular vibrational excitation, phonon (intermolecular vibration) excitation, rotational excitation, and elastic scattering were considered (Matsuya *et al* 2021). The interactions related to the chemical products are ionization, excitation, and DEA (which is described in the below section 2.2). The electron cutoff energy of the *PHITS-ETS* mode has to be set lower than 4.3 eV, which corresponds to the lowest energy of the DEA cross section (Matsuya *et al* 2021). We reduced the DEA cross-section of gas phase (Itikawa & Mason 2005) by a factor of 1/6 because only a negligible DEA frequency in an aqueous solution has been reported (Wang *et al* 2009). In the *PHITS-ETS* mode, the minimal cut-off energy is 1 meV. The transport of electrons down to thermal energies was validated by comparing results obtained by the *PHITS-ETS* mode to experimental values reported elsewhere (Konovalov *et al* 1988). However, because scientific data of thermal energy electrons is insufficient, it is needed to further investigate the low-energy electrons in a future study. Therefore, it is sufficient to set the cut-off energy to 1 eV when using the *PHITS-Chem* code because it uses a correction model for the spatial distribution of the thermalized electrons to reduce the calculation time. To obtain the three-dimensional coordinates and the type of atomic interactions, we used a tally named “t-userdefined” that allows the output of any physical quantity that cannot be output by the other tallies in the default setting of PHITS.

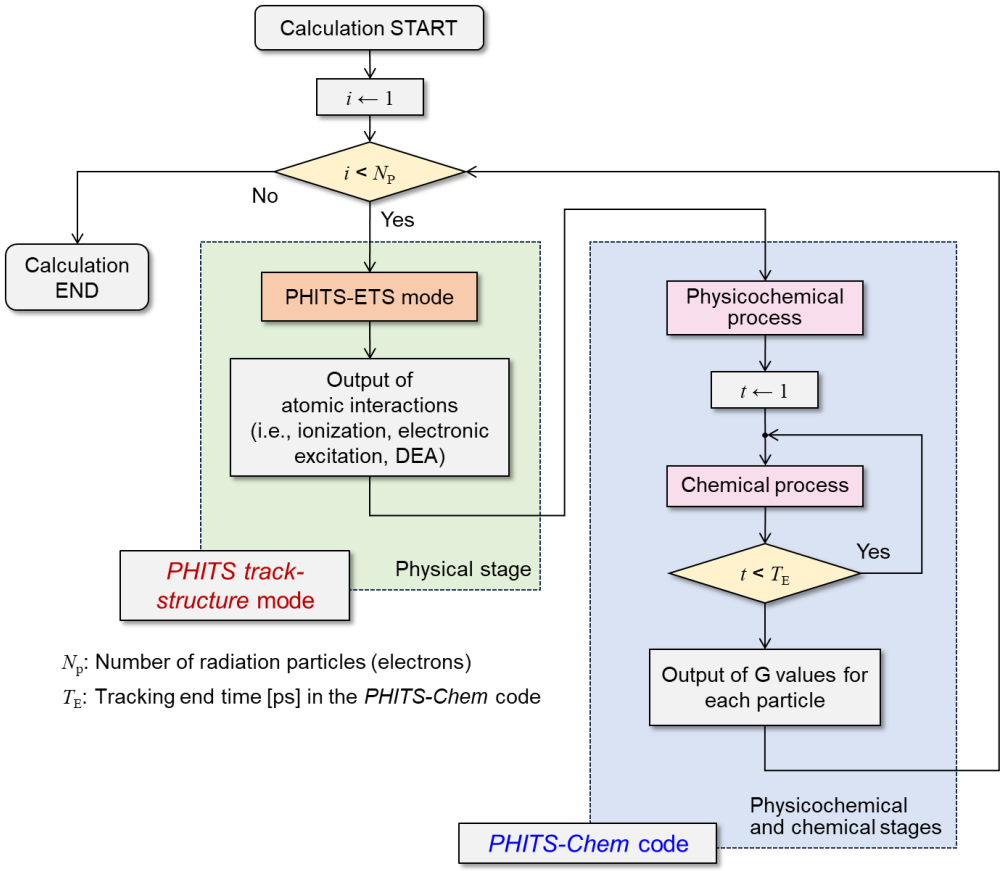

Figure 1. Simulation flow of physical and chemical stages in the PHITS code. In this simulation system, PHITS track-structure simulation has to be performed first to output coordinates and types of atomic interactions (physical stages by the *PHITS-ETS* mode), and then physicochemical and chemical stage simulations (the *PHITS-Chem* code) can be performed by reading the output data into an external chemical code.

2.2. Physicochemical stage

In the physicochemical stage, the product H_2O^+, H_2O^-, and H_2O^* can be immediately converted into other molecular products. However, little is known about the quantitative and qualitative production procedure of chemical species starting from each excited state of water molecule. There are several types of dissociation schemes (Turner *et al* 1988, Tomita *et al* 1997, Hamm *et al* 1989, Hill & Smith 1994, Kreipl *et al* 2009, Uehara & Nikjoo 2006, Shin *et al* 2021, Baba *et al* 2021). Recently, initial yields at time after irradiation within 300 fs has been proposed based on the origin of the *PHITS-ETS* mode (so called dynamic Monte Carlo code (DMCC)) (Kai *et al* 2023), which can reproduce the experimental initial yields of e_{aq}^-. Based on the previous studies, we made the different assumption on the branching ratios in order to produce consistent initial yields (G value at 1 ps) for various radical species (see Table 1). Note that the branching ratios listed in Table 1 is a new model dedicated to the PHITS code and a part of the *PHITS-Chem* code that is not considered in *PHITS-ETS* mode.

Table 1. Dissociation scheme and associated probability in the *PHITS-Chem* code

Physical type	Decay Channel	Fraction (%)
Ionization		
$1b_1$, $3a_1$, $1b_2$, $2a_1$, $1a_1$	$H_3O^+ + {}^{\bullet}OH + e^-$	100.0
Electronic excitation		
A^1B_1	$H^{\bullet} + {}^{\bullet}OH$	75.0
	$H_2 + {}^{\bullet}O^{\bullet}$	25.0
B^1A_1	$H^{\bullet} + {}^{\bullet}OH$	50.0
	$H_2 + H_2O_2$	50.0
Rydberg	$H^{\bullet} + {}^{\bullet}OH$	100.0
diff bands	$H_3O^+ + {}^{\bullet}OH + e^-$	90.0
	$H^{\bullet} + {}^{\bullet}OH$	10.0
Collective	$H_3O^+ + {}^{\bullet}OH + e^-$	100.0
Dissociative electron attachment		
OH^- production	$H^{\bullet} + OH^-$	3.0
O^- production	$O^- + H_2$	11.5
H^- production†	${}^{\bullet}OH + H_2 + OH^-$	11.4
	${}^{\bullet}OH + 2H^{\bullet} + OH^-$	74.1

† $H_2O + e^- \rightarrow H_2O^- \rightarrow H^- + {}^{\bullet}OH$, and $H_2O + H^- \rightarrow H_2$ (or $2H^{\bullet}$) + OH^-

The branching ratios are listed in Table 1. All ionizations ($1b_1$, $3a_1$, $1b_2$, $2a_1$, $1a_1$) were assumed to produce H_2O^+ cations following decay of $H_2O^+ + H_2O \rightarrow H_3O^+ + {}^{\bullet}OH$ (Hamill 1969). The displacement of H_2O^+ from the ionization site is sampled from a Gaussian distribution with a mean displacement of 1.25 nm (Tomita *et al* 1997). The H_3O^+ was assumed to be at the same position as the H_2O^+ and the ${}^{\bullet}OH$ is positioned with random orientation at a mean distance of 0.29 nm (Uehara & Nikjoo 2006, Tomita *et al* 1997). Like ionizations, 100% collective excitation and 90% diffuse band excitation were assumed to produce H_3O^+ and ${}^{\bullet}OH$, because the excitations can release secondary electrons (Kai *et al* 2023). In the dissociation of an excited water molecule into $H^{\bullet}$ and ${}^{\bullet}OH$ radicals, the products were assumed to be separated by 0.87 nm on a randomly oriented line centered at the excitation site (Tomita *et al* 1997, Uehara & Nikjoo 2006), and as well as in the case of H_2 and O by 0.58 nm (Tomita *et al* 1997). The rest 10% of diffuse band excitation was also assumed to be excited state A^1B_1. The two H atoms are positioned at 0.8 nm from the O atom (Cobut *et al* 1998). The production positions of these radicals follow a Gaussian distribution with a standard deviation (s.d.) that has been modelled in other simulation codes (Kreipl *et al* 2009, Bernal *et al* 2015). Furthermore, the dissociation scheme of the DEA and the associated probabilities are also listed in Table 1. The DEA scheme remains uncertain as well as the role of inducing DNA damage (in water solution). In this regard, we assumed the three branches, namely, OH^-, O^-, and H^- productions (Matsuya *et al* 2021). The percentages of three production pathways correspond to the ratios of integral cross sections of three types of DEA (i.e., 3% for OH^- (4.3 eV), 11.5% for O^- (4.43 eV) and 85.5% for H^- (5.5 eV)). Based on the previous models (Bernal *et al* 2015), we assumed that H^- radicals can immediately react with to H_2O and generate H_2 (or 2 $H^{\bullet}$), and OH^- ($H_2O + e^- \rightarrow H_2O^- \rightarrow H^- + {}^{\bullet}OH$, and $H_2O + H^- \rightarrow H_2$ (or $2H^{\bullet}$) + OH^-) as shown in Table 1. Note that the DEA scheme was designed to reproduce the initial yields of minor products such as H_2, $H^{\bullet}$, O^-, and OH^-, so when the role is clarified, there is a

possibility to revise the scheme in the future.

Electrons with kinetic energy less than the 7 eV (here called subexcitation electron (e_{sub}^-)) thermalize losing their energy by molecular excitations (such as vibrational, rotational and photon excitations), leading to the formation of hydrated electrons e_{aq}^-. The cutoff energy must be set in the PHITS code in the same manner as other Monte Carlo codes. The full simulation of electrons down to 10^{-3} eV allows the estimation of the position of e_{aq}^-; however, the computational time is very long. We then used a model for the thermalization distance. The thermalization distance depends on the cut-off energy. In this model, assuming that the multi-step thermalization process can be approximated by a single-step motion traveling the mean thermalization distance in a random direction and its s.d. (Terrissol & Beaudre 1990, Uehara & Nikjoo 2006). Based on those studies, the thermalization distance r (nm) as a function of the cutoff energy e_{cut} can be approximately expressed as $r = 3.151 + 0.964\ e_{cut} + 1.362\ e_{cut}^2 - 0.134\ e_{cut}^3$ with its uncertainty of ± 50%. In general, the e_{sub}^- can recombine their parent cations (with ~4% of all ionizations) (Uehara & Nikjoo 2006), which is well known as electron-hole recombination ($e_{sub}^- + H_2O^+ \rightarrow H_2O^*$). The excited water molecule is assumed to be reorganized as excited state H_2O^* (Beaudre 1988). However, in the *PHITS-ETS* mode, the recombination of e_{sub}^- with their cations has already been considered in the track-structure model based on the DMCC code (Kai *et al* 2023). Therefore, the *PHITS-Chem* code does not require an empirical model for recombination.

2.3. Chemical stage

In the chemical stage, using an SBS approach, the *PHITS-Chem* code enables the simulation of chemical reactions 10^{-12} s after irradiation. This SBS approach is time-consuming; however, it enables the calculation of the positions of all species at all times. The details of the chemical model are described below.

The timestep τ of chemical reactions in the PHITS-Chem code is a constant value of 1 ps. During each time step of τ, water radiolytic species and their products were allowed to diffuse randomly. The diffusion coefficients D for the 16 species are listed in Table 2, in which most of the values were obtained from the previous chemical code (Tomita *et al*. 1997, Uehara & Nikjoo 2006). In the chemical model, the reactions of the chemical products to H_2O and OH radical scavengers are considered using the reaction rate constant listed in Table 3. During the simulation, the root-mean-square distance traveled λ was calculated following $\lambda = \sqrt{6D\tau}$, and the actual distance was determined sampling a Gaussian with 10% s.d. (Uehara & Nikjoo 2006). After diffusion for each time step of τ, the pair of species closer than their reaction radius can be replaced by the reaction products. We calculated the reaction radius a (nm) for each pair of interacting species A and B, following the relationship $a = k/4\pi(D_A+D_B)$, where k is the reaction rate constant (neutral pH, 1 atm, 25°C) listed in Table 3 (Tomita *et al*. 1997, Uehara & Nikjoo 2006). Using a value calculated from the k value (listed in Table 3), the reaction was performed if the distance between A and B (D_A+D_B) is shorter than $2a$ (Uehara & Nikjoo 2006). As shown in Table 3, 16 species and 35 chemical reactions including the scavenging processes of $^{\bullet}OH$ by Tris and DMSO (Tomita *et al*. 1997). By considering the chemical

reaction of the OH radical scavenger, this code has the advantage of analyzing DNA damage induction mechanisms by indirect effects.

Table 2. Chemical species and value of diffusion coefficients *D* in the *PHITS-Chem* code

Species	D ($\times 10^{-9}$ m^2 s^{-1})	Reference	Note (previous chemical code)
e_{aq}^-	4.5	Uehara & Nikjoo 2006	KURBUC code
$^{\bullet}OH$	2.8	Tomita *et al.* 1997, Uehara & Nikjoo 2006	DBREAK system, KURBUC code
$H^{\bullet}$	7.0	Tomita *et al.* 1997, Uehara & Nikjoo 2006	DBREAK system, KURBUC code
H_3O^+	9.3	Tomita *et al.* 1997	DBREAK system
H_2	5.0	Tomita *et al.* 1997, Uehara & Nikjoo 2006	DBREAK system, KURBUC code
H_2O_2	2.3	Tomita *et al.* 1997	DBREAK system
HO_2	2.0	Tomita *et al.* 1997	DBREAK system
O_2	2.4	Tomita *et al.* 1997	DBREAK system
OH^-	5.0	Tomita *et al.* 1997, Uehara & Nikjoo 2006	DBREAK system, KURBUC code
O_2^-	2.1	Tomita *et al.* 1997, Uehara & Nikjoo 2006	DBREAK system, KURBUC code
HO_2^-	1.4	Tomita *et al.* 1997	DBREAK system
$^{\bullet}O^{\bullet}$	2.0	Tomita *et al.* 1997	DBREAK system
O^-	2.8	Tomita *et al.* 1997	DBREAK system
tris	1.0	Tomita *et al.* 1997	DBREAK system
DMSO	1.1	Tomita *et al.* 1997	DBREAK system
H_2O	0.0	Tomita *et al.* 1997	DBREAK system

2.4. OH radical scavenger model

In the *PHITS-Chem* code, we adopted the SBS approach for simulating radiolysis (Plante & Devroye 2017). When considering the radical scavengers following the SBS approach, it is needed to consider the spatial positions of the scavengers (i.e., Tris and DMSO). However, when considering individual scavengers within the whole water (e.g., a water sphere with 61.8 μm that at least 1% of the electron kinetic energy was deposited in this region), the generation of the scavengers in the case of the high scavenging capacity exceeds the memory of the computer. In this study, we developed a model for OH radical scavengers that reduces the need for computer memory.

In the physicochemical model, the scavengers were generated along the track to save the computation memory. In detail, first, the initial coordinates of OH radicals at 1 ps were detected and the space along the track was divided into 3D grids (i.e., $50 \times 50 \times 50$ nm^3). Second, depending on the scavenger capacity, the scavengers were generated inside one segment. Recording the coordinates of the radical scavengers for all segments exceeds the computer memory. Thus, the coordinates of the scavengers in one segment were memorized during the simulation and were used for the subsequent chemical simulation.

In the chemical model, the diffusions of the radical scavengers in one segment were considered using the diffusion coefficients *D* of Tris and DMSO (see Table 2). In addition to the physicochemical model, to save the computer memory further, the coordinates after the diffusion inside one segment for each timestep (in other words, the spatial distribution of the scavengers memorized in the physicochemical stage calculation) were used for each segment divided in the physicochemical stage

calculation. This technique can significantly reduce the computer memory and realize the SBS simulation of radical scavengers even for the case of high scavenging capacity such as 10^{10} s^{-1}. In the same manner as the other chemical species, using *a* value calculated from the *k* value (see Table 3), the reaction was performed if the distance between A and B (D_A+D_B) is shorter than 2*a*.

Table 3. Chemical reactions and value of reaction rate constants *k* and radius *a*

Reaction (A + B)				Products			*k* (10^{10} dm^3 mol^{-1} s^{-1})	*a* (nm)
$^{\bullet}OH$	+	$^{\bullet}OH$	→	H_2O_2			0.550	0.129
e_{aq}^-	+	e_{aq}^-	→	H_2	+	$2OH^-$	0.500	0.0734
$H^{\bullet}$	+	$H^{\bullet}$	→	H_2			1.000	0.0944
$^{\bullet}OH$	+	e_{aq}^-	→	OH^-			2.50	0.453
$^{\bullet}OH$	+	$H^{\bullet}$	→	H_2O			2.00	0.270
H_3O^+	+	OH^-	→	H_2O			14.3	1.32
$H^{\bullet}$	+	H_2O_2	→	$^{\bullet}OH$			0.0160	0.00227
e_{aq}^-	+	H_3O^+	→	$H^{\bullet}$			1.70	0.163
e_{aq}^-	+	$H^{\bullet}$	→	H_2	+	$^{\bullet}OH$	2.50	0.287
e_{aq}^-	+	O_2	→	O_2^-			1.90	0.364
e_{aq}^-	+	O_2^-	→	OH^-	+	HO_2^-	1.30	0.260
e_{aq}^-	+	HO_2	→	HO_2^-			2.00	0.407
$H^{\bullet}$	+	$^{\bullet}O^{\bullet}$	→	$^{\bullet}OH$			2.00	0.294
$H^{\bullet}$	+	O_2	→	HO_2			1.90	0.267
$H^{\bullet}$	+	O_2^-	→	HO_2^-			2.00	0.290
$H^{\bullet}$	+	HO_2	→	H_2O_2			2.00	0.294
H_3O^+	+	O_2^-	→	HO_2			3.80	0.441
$^{\bullet}O^{\bullet}$	+	$^{\bullet}O^{\bullet}$	→	O_2			2.20	0.727
$^{\bullet}OH$	+	$^{\bullet}O^{\bullet}$	→	HO_2			2.00	0.551
$^{\bullet}O^{\bullet}$	+	HO_2	→	$^{\bullet}OH$	+	O_2	2.00	0.661
$^{\bullet}OH$	+	O_2^-	→	O_2	+	OH^-	1.20	0.324
$^{\bullet}OH$	+	HO_2	→	O_2			1.20	0.330
$^{\bullet}OH$	+	OH^-	→	O^-			1.30	0.220
$H^{\bullet}$	+	OH^-	→	e_{aq}^-			0.00210	0.000231
$^{\bullet}OH$	+	H_2O_2	→	HO_2			0.00330	0.000855
$^{\bullet}OH$	+	O^-	→	HO_2^-			1.80	0.425
$^{\bullet}OH$	+	HO_2^-	→	HO_2	+	OH^-	0.750	0.236
e_{aq}^-	+	HO_2^-	→	$2OH^-$	+	H_2	0.350	0.0784
e_{aq}^-	+	O^-	→	OH^-	+	OH^-	2.20	0.398
$H^{\bullet}$	+	O^-	→	OH^-			2.00	0.270
H_3O^+	+	O^-	→	OH			5.00	0.546
H_3O^+	+	HO_2^-	→	H_2O_2			5.00	0.618
$^{\bullet}OH$	+	Tris	→	scavenged			0.150	0.0522
$^{\bullet}OH$	+	DMSO	→	scavenged			0.660	0.224
HO_2	+	O_2^-	→	O_2	+	HO_2	1.00	0.300

2.5. Benchmark test of the chemical code

To verify the chemical code developed in this study, we simulated the time-dependent G values of major products (i.e., $^{\bullet}OH$, e_{aq}^-, H_2, H_2O_2) under the exposure to electrons with kinetic energy of 1 MeV, and compared them to the experimental values (Buxton 1972, Wolff *et al* 1973, Johna *et al* 1973 1976 1977, Draganic & Draganic 1975, Sumiyoshi & Katayama 1982, Belloni *et al* 1983, LaVerne & Pimblott 1991, Pastina & LaVerne 1999, Bartels *et al* 2000, LaVerne 2000; Muroya *et al* 2005; Wang

et al 2018) and other simulation results (Tomita *et al* 1997, Pimblott & LaVerne 1997, Kreipl *et al* 2009, Uehara & Nikjoo 2006, Shin *et al* 2021, Baba *et al* 2021). In this benchmark test, the *PHITS-ETS* mode was activated in a water sphere positioned at the origin in the PHITS simulation world. We used the electron gamma shower EGS mode (Hirayama *et al* 2005) in the region outside the water sphere. The cutoff energies of the electrons inside and outside of the water sphere were set as 1 eV and 1 keV, respectively. 1 MeV electrons were generated at the origin and simulated in the water sphere whose center was located at the origin (see Fig. S2 in *supplementary file*). The radius of the water sphere was set to be 61.8 μm. The radius was defined to be sufficiently large that at least 1% of the electron kinetic energy was deposited in this region. The chemical simulation based on SBS approach is a time-consuming calculation, so we simulated more than 50 independent electron tracks.

We also calculated the primary yields of •OH, e_{aq}^-, and H_2O_2 (G values at 1 μs after irradiation) for various incident electron energies. In this calculation, the electrons were transported until they were fully stopped within liquid water. The estimated primary yields were compared with previous simulations using DBREAK system (Tomita *et al* 1997, Watanabe *et al* 2021). In addition, we calculated the dynamics of •OH for various scavenging capacities (i.e., 0, 10^6, 10^7, 10^8, 10^9, and 10^{10} s^{-1}) of Tris. From the calculations, we verified the performance of this chemical code for OH radical scavenging.

2.6. DNA damage analysis using this chemical code

To test the applicability of this chemical code for biological study, we also applied the *PHITS-Chem* code for DNA damage analysis. To analyze the relationship between DNA damage yields and G values, we first obtained electron spectra generated by 150 kVp X-rays using the EGS mode and transported the electrons until they were fully stopped within the actual dimension of the sphere using the *PHITS-ETS* mode assuming secondary electron equilibrium. The reason why we adopted the electron spectrum is that the experimental yields of various DNA damage types are available under the irradiation condition of 150 kVp X-rays (Shiina *et al* 2013). Second, we calculated the time-dependent G value of •OH from 1 ps to 1 μs under various scavenging capacities c_{SCA} (i.e., 10^6–10^{10} s^{-1}) and calculated the time-integral G value for a certain scavenging capacity ($G_{INT}(c_{SCA})$ [/100 eV]) using the following equation,

$$G_{INT}(c_{SCA}) = \int G(c_{SCA}, t)\mathrm{d}t \quad (1)$$

where $G(c_{SCA}, t)$ is the G value of •OH at time t (s) after irradiation for certain scavenging capacity c_{SCA}. The G value of •OH at 1 μs under 150 kVp X-rays is lower than 0.6 per 100 eV, and it takes a long calculation time to obtain G value of •OH at 1 μs. Considering these, as an application example, we decided to integrate the G values from 1 ps to 1 μs in this study.

We assumed that total DNA damage yields $Y_{DE\&IDE}$ are composed of the yield by direct effects (DE) Y_{DE}, that is independent on scavenging capacity c_{SCA}, and that by indirect effects (IDE) as a function of scavenging capacity $Y_{IDE}(c_{SCA})$. Using the $G_{INT}(c_{SCA})$ (given by Eq. (1)), we calculated the

total yields as a function of scavenging capacity $Y_{DE\&IDE}(c_{SCA})$ for various types of DNA damage, that is, the single-strand break (SSB), the double-strand break (DSB), the base damage (BD), and the apurinic/apyrimidinic (AP) site following the steps.

1) The value of Y_{DE} for each DNA damage was approximately determined from the yield in the presence of Tris with 10^{10} s^{-1} scavenging capacity ($Y_{DE} = Y_{DE\&IDE}(10^{10})$), based on the experimental report (Shiina *et al* 2013).
2) The $Y_{IDE}(c_{SCA}=10^6)$ value for each damage type was obtained by subtracting the Y_{DE} (obtained by step No. 1) from total yields ($Y_{DE\&IDE}(c_{SCA}=10^6)$). We then determined the coefficient of the $G_{INT}(c_{SCA})$ to calculate the $Y_{IDE}(c_{SCA})$ (η in 100 eV/Gy/Da) by dividing the $Y_{IDE}(10^6)$ by $G_{INT}(10^6)$.
3) Using the Y_{DE}, $G_{INT}(c_{SCA})$, and η, the total yields $Y_{DE\&IDE}(c_{SCA})$ for each DNA damage type by the following formula.

$$Y_{DE\&IDE}(c_{SCA}) = Y_{DE} + Y_{IDE}(c_{SCA}) = Y_{DE} + \eta G_{INT}(c_{SCA}) \quad (2)$$

Using Eq. (2), we estimated the yields of various DNA damage types (i.e., SSB, DSB, BD, and AP site) as a function of scavenger capacity, and compared the estimated yields with the experimental data (Fulford *et al* 2001, Shiina *et al* 2013) and other simulation values (Fulford *et al* 2001). It should be noted that these experimental values were measured using pUC18 plasmid DNA (Fulford *et al* 2001, Shiina *et al* 2013), whereas we calculated the yields using the simple formula (see Eq. (2)) without considering DNA type.

3. RESULTS AND DISCUSSIONS

3.1. Verification of the chemical code for PHITS

Figure 2 shows the time dependence of the (A) •OH, (B) e_{aq}^-, (C) H_2, and (D) H_2O_2 yields, where the G values estimated by PHITS (blue circle) were compared to the experimental values (Buxton 1972, Wolff *et al* 1973, Johna *et al* 1973 1976 1977, Draganic & Draganic 1975, Sumiyoshi & Katayama 1982, Belloni *et al* 1983, LaVerne & Pimblott 1991, Pastina & LaVerne 1999, Bartels *et al* 2000, LaVerne 2000; Muroya *et al* 2005; Wang *et al* 2018) and other simulation results (Tomita *et al* 1997, Pimblott & LaVerne 1997, Kreipl *et al* 2009, Uehara & Nikjoo 2006, Shin *et al* 2021, Baba *et al* 2021). From Fig. 1, the PHITS simulation shows that the initial yields of •OH, and e_{aq}^- are 5.12 and 4.50, respectively, and the dynamics of •OH, e_{aq}^-, H_2, and H_2O_2 are similar to the experimental data and other simulation results. Amongst the comparisons, the G value of H_2O_2 calculated using the *PHITS-Chem* code was lower than the measured data and other simulation results. The experimental G values were measured using high-energy electrons with $\geq$ 1 MeV electrons or γ-rays, whereas the PHITS simulation selected 1 MeV mono-energetic electrons. The stopping power, which is intrinsically related to the intra-spur distance, depends on the kinetic energy of the electron (Matsuya *et al* 2019). Considering the subtle differences in electron energy between simulation and experiments, the accuracy of the *PHITS-Chem* code was found to be good. In the *PHITS-Chem* code, the SBS

approach with a constant timestep of 1 ps, leading to long calculation time when calculating the G values at 1 μs. Other codes, e.g., PARTRAC, uses variable time steps (Kreipl *et al* 2009). As one of the future developments, the variable time steps can reduce the computational time of the *PHITS-Chem* code.

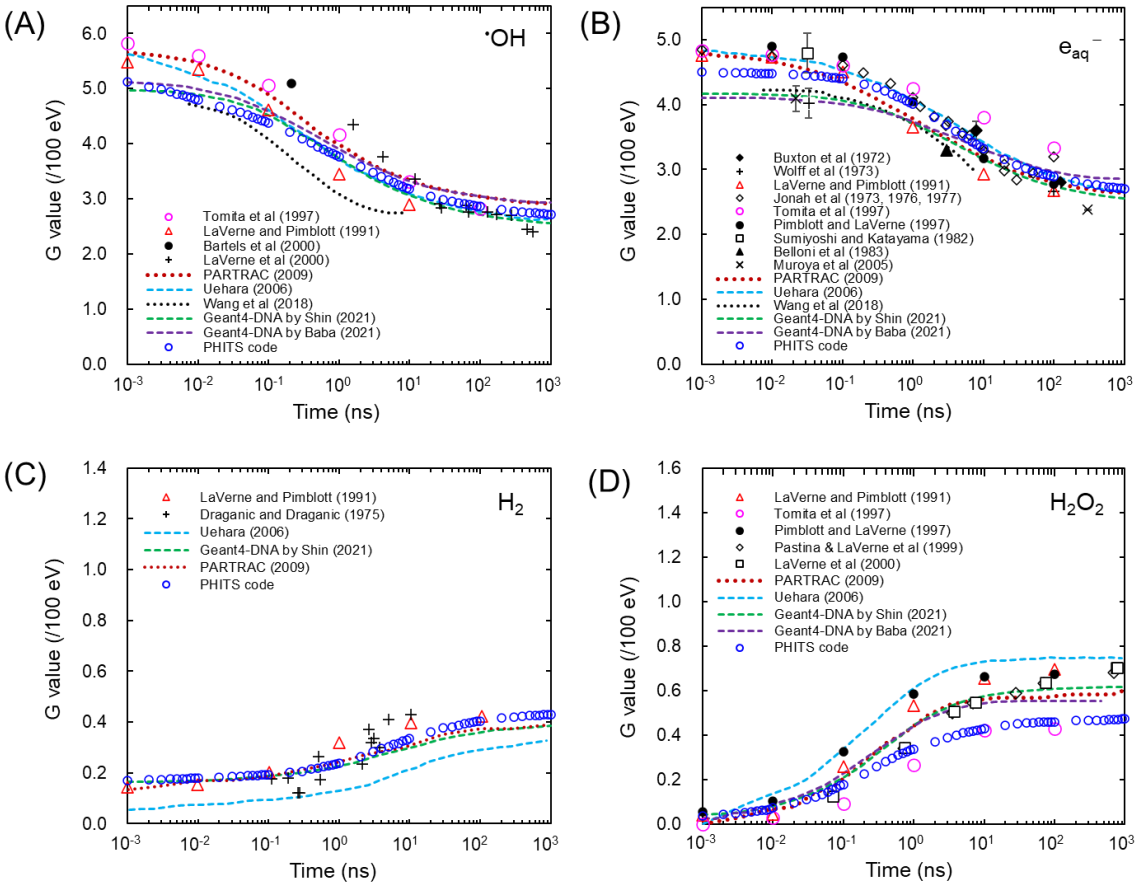

Figure 2. Time dependence of the (A) ·OH, (B) e_{aq}^-, (C) H_2, and (D) H_2O_2 yields. In the PHITS physical simulation, atomic interactions under 1 MeV electrons were simulated, and the energy deposition was approximately 1% of the electron kinetic energy. Note that the simulation timestep is a constant value of 1 ps and the *PHITS-Chem* simulation data were thinned out to a factor 10 per decade. The G values calculated using PHITS were compared with the experimental values (Buxton 1972, Wolff *et al* 1973, Johna *et al* 1973 1976 1977, Draganic & Draganic 1975, Sumiyoshi & Katayama 1982, Belloni *et al* 1983, LaVerne & Pimblott 1991, Pastina & LaVerne 1999, Bartels *et al* 2000, LaVerne 2000; Muroya *et al* 2005; Wang *et al* 2018) and other simulation results (Tomita *et al* 1997, Pimblott & LaVerne 1997, Kreipl *et al* 2009, Uehara & Nikjoo 2006, Shin *et al* 2021, Baba *et al* 2021).

3.2. Characteristics of the PHITS chemical code

The estimated G-values of ·OH, e_{aq}^-, H_2O_2, H·, and O as a function of the incident electron energy are depicted in Fig. 3, where (A) is the initial yields (G values at 1 ps) and (B) is the primary yields (G values at 1 μs). The PHITS simulation (dotted lines) was compared to previous simulation results (Tomita *et al* 1997, Watanabe *et al* 2021, Uehara & Nikjoo 2001). As shown in Fig. 3(A), the initial yields of the four products (·OH, e_{aq}^-, H·, and O) calculated by the PHITS code agreed well with the other simulation results. The PHITS results showed almost the same initial yields of ·OH as the recent estimation using Geant4-DNA (Shin *et al* 2021). Meanwhilst, as shown in Fig. 3(B), the

primary yields of three products (•OH, e_{aq}^-, and H_2O_2) calculated by PHITS were in reasonable agreement with other simulation results for the electron energies higher than 1 keV. However, there are some differences in the energy range of < 1 keV compared with the DBREAK system (Watanabe *et al* 2001). This difference is due to the unique cross-sections of molecular excitations in the *PHITS-ETS* mode, which was developed based on the DMCC (Kai *et al* 2015a, 2015b). Considering these comparisons (Figs. 2 and 3), it was verified that the *PHITS-Chem* code could reproduce the chemical product yields as functions of both time after irradiation and incident electron energy.

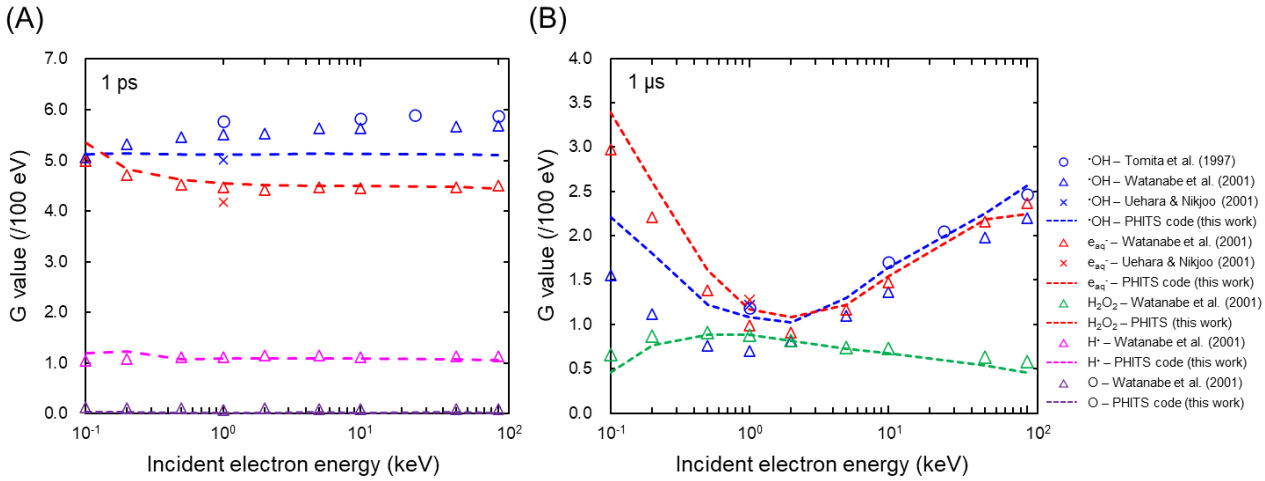

Figure 3. Initial and primary yields as a function of incident electron energy. (A) is initial yields (G values at 1 ps) of four products (such as •OH, eaq–, H•, and O) and the primary yields (G values at 1μs) of three products (such as •OH, e_{aq}^-, and H_2O_2). In the PHITS physical simulation, the entire kinetic energy of the electrons was absorbed in liquid water. The PHITS simulations were compared with the previous simulation results (Tomita *et al* 1997, Watanabe *et al* 2021, Uehara & Nikjoo 2001).

An advantage of the *PHITS-Chem* code is the time dependence of the G values in the presence of •OH radical scavengers, such as Tris and DMSO. Figure 4 shows the time course of •OH under various scavenging capacities (i.e., 0, 10^6, 10^7, 10^8, 10^9, and 10^{10} s^{-1}). As shown in Fig. 4, the G value of •OH decreased with increasing scavenging capacity. The dynamics estimated by the *PHITS-Chem* code are based on the SBS approach, which is time-consuming but calculates the positions of all species at all times. As a preliminary test, we compared the G values for each track (PHITS simulation) to those calculated by the DBREAK system (Tomita *et al* 1997), as described in Fig. S3 in the *Supplementary file*. In the test, the •OH calculated using the DBREAK system decreased more quickly than the PHITS calculation. This is because the *PHITS-Chem* simulation adopts a single-track calculation, whereas the G value by the DBREAK system was calculated for the case of 100 Gy. In general, chemical reactions in the inter-tracks are induced by high-dose radiation. Therefore, the G value calculated using the DBREAK system is lower than that calculated using the *PHITS-Chem* code.

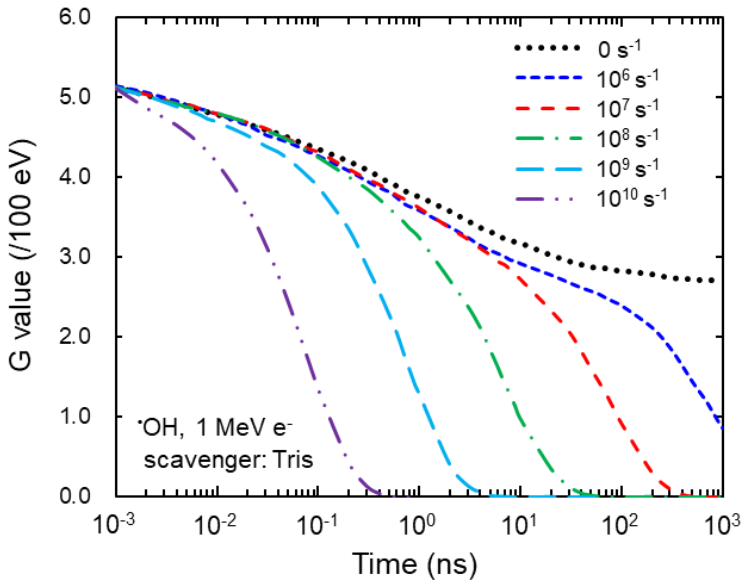

Figure 4. Time dependence of OH in the presence of OH radical scavengers. The scavenging capacities were set to be 0, 10^6, 10^7, 10^8, 10^9, and 10^{10} (1/s). In the PHITS physical simulation, atomic interactions under 1 MeV electrons were simulated, and the energy deposition was approximately 1% of the electron kinetic energy in the same manner as Fig. 2.

3.3. Application of this chemical code to DNA damage analysis

Finally, we applied the *PHITS-Chem* code to DNA damage analysis. Figure 5 shows the relationship between scavenging capacity and the yields of DNA lesions, where lines and symbols represent the estimated yields and the experimental values (Fulford *et al* 2001, Shina et al 2013). When estimating the DNA damage yields, we used the electron energy spectrum of 150 kVp X-rays, which was depicted in Fig. S4 in *Supplementary Material*. The coefficients η for SSB, DSB, BD, and AP site were 7.65×10^{-15}, 1.37×10^{-16}, 1.16×10^{-14}, and 4.09×10^{-15}, respectively. The Y_{DE} values for the SSB, DSB, BD, and AP site were obtained as 1.90×10^{-10}, 1.60×10^{-11}, 8.20×10^{-10}, and 9.70×10^{-11}, respectively. As shown in Fig. 5, regardless of the DNA damage type, the indirect effects of OH radicals (G) were proportional to the yields of all DNA lesions (i.e., SSB, DSB, BD, and AP site) in the range of scavenging capacity 10^6–10^7 s^{-1}. In this regard, this chemical simulation suggests that indirect effects play an important role in DNA damage induction at a low scavenging capacity of < 10^7 s^{-1}. Meanwhilst, the direct effects are the main cause of DNA lesions at high scavenging capacity of > 10^7 s^{-1}. The contribution of OH radicals to DNA damage induction can be discussed using the *PHITS-Chem* code.

As shown in Figs. 3 and 4, the *PHITS-Chem* code in PHITS can simulate the time-dependent yields of chemical products resulting from water radiolysis as functions of the electron energy and scavenging capacity of OH radicals. It has been known that scavenging capacity in mammalian cells is higher than that of the pure liquid water, i.e., 3×10^8 s^{-1} (Fulford *et al* 2001). Thus, the contribution of chemical products to DNA damage induction can be discussed using this chemical code considering their scavenging capacity. In contrast to OH radicals, the lifetime of e_{aq}^- with OH radical scavengers can be longer than that without the scavenger, because the number of $^{\bullet}OH + e_{aq}^-$ reactions decreases in

the presence of OH radical scavengers. A clustered DNA lesion, defined as multiple DNA lesions induced within a 10-bp separation, might be mainly influenced by OH radical scavengers (Tomita *et al* 1998). Meanwhilst, our previous modelling of DNA damage estimation suggested that analyzing the spatial distribution of ionizations and electronic excitations is sufficient to estimate DNA damage yields without any chemical simulations (Matsuya *et al* 2019, 2020, 2021, 2022). Considering the SSB and DSB yields under the cell condition (i.e., 3×10^8 s^{-1}), the contribution of the indirect effects seems to be smaller than that in the pure liquid water (i.e., $\leq 1 \times 10^6$ s^{-1}). As shown in Fig. 5, this chemical code would be useful for proving our modelling and mechanistically evaluating the impacts of indirect effects on DNA damage induction in the human body. However, it is essential to consider the reaction rate constant, *k*, of OH radicals with DNA in chemical simulations. Further development and modeling should be conducted in future studies.

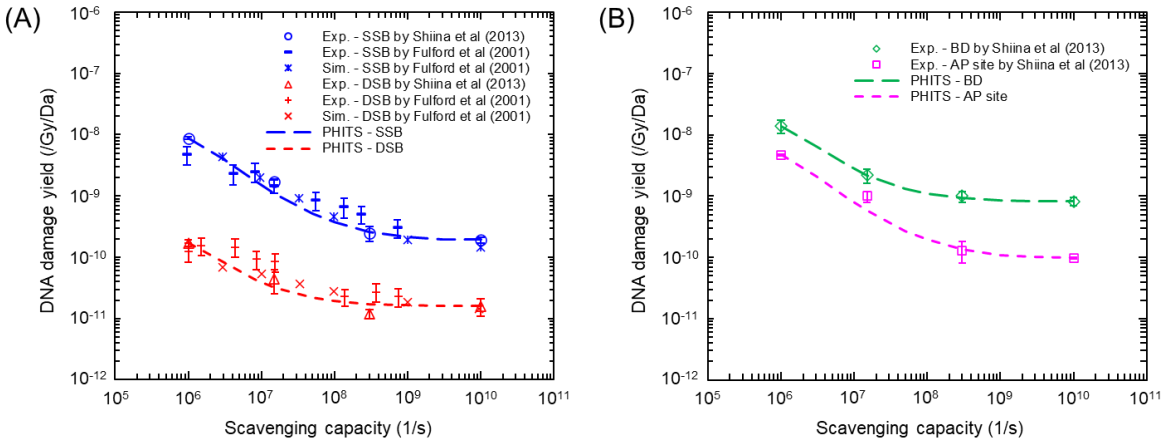

Figure 5. DNA damage yields and time-integral G-values of OH radicals as a function of scavenging capacity of Tris. The G values were integrated from 10^{-12} to 10^{-6} sec, and the relationship between the time integral G-value and the experimental DNA damage yields (Fulford *et al* 2001, Shiina *et al* 2013) was depicted.

4. CONCLUSIONS

In this study, we developed a chemical code dedicated to PHITS (*PHITS-Chem* code), that allows the calculation of the G values of 16 products (e.g., $^{\bullet}OH$, e_{aq}^-, H_2, and H_2O_2) and 35 chemical reactions as a function of time after irradiation ($\geq$ 1 ps). The calculated G values of the major products $^{\bullet}OH$, e_{aq}^-, H_2, and H_2O_2 for the interval from 1 ps to 1 μs agreed well with typical data (i.e., experimental data and other simulation results). Amongst the chemical reactions, the two types of OH radical scavengers (i.e., Tris and DMSO) are considered in this chemical code and found to be useful for discussing the induction mechanisms of various DNA lesions such as SSB, DSB, BD, and AP site. The *PHITS-Chem* code would be useful for evaluating the relationship between the direct and indirect effects of radiation exposure. The *PHITS-Chem* code is currently designed to be used in combination with *PHITS-ETS* mode. In the PHITS code, the ion track-structure mode, well known as the *PHITS-KURBUC* mode (Matsuya *et al* 2021), is available, so further development of the chemical code to handle proton- and carbon-induced chemical species is required in the near future. This

PHITS-Chem code will be included and make available in the future version of the PHITS code.

CONFLICT OF INTEREST

The authors declare that they have no conflict of interest.

FUNDING

This work was supported by the Japan Society for the Promotion of Science KAKENHI (Grant no. 22H03744, 22K04993, 23K04635).

AUTHOR CONTRIBUTIONS

Y. Matsuya, Y. Yoshii, T. Kai designed this study. Y. Matsuya and Y. Yoshii developed this chemical code. Y. Matsuya, Y. Hirata and T. Kai improved the PHITS track-structure mode. Y. Matsuya and T. Kusumoto discussed the G values of products by water radiolysis and compared to the experiments and other simulation results. T. Sato and T. Kai supervised this study. Y. Matsuya wrote the manuscript. All authors reviewed the manuscript.

REFERENCES

Baba K, Kusumoto T, Okada S, Ogawara R, Kodaira S, Raffy Q, Barillon R, Ludwig N, Galindo C, Peaupardin P, Ishikawa M 2021 Quantitative estimation of track segment yields of water radiolysis species under heavy ions around Bragg peak energies using Geant4-DNA. *Sci Rep.* 11, 1524.

Bartels DM, Cook AR, Mudaliar M, Jonah CD 2000 Spur decay of the solvated electron in picosecond radiolysis measured with time-correlated absorption spectroscopy, *J. Phys. Chem. A* 104, 1686–1691.

Beaudre A 1988 These de l'Universite Paul Sabatier, Toulouse, France, no. 371.

Belloni J, Billiau F, Delaire JA, Delcourt MO, Marignier JL 1983 Ionizing radiationliquid interactions: a comparative study of polar liquids, *Radiat. Phys. Chem.* 21, 177–183.

Bernal MA, Bordage MC, Brown JMC, Davídková M, Delage E, El Bitar Z, Enger SA, Francis Z, Guatelli S, Ivanchenko VN, Karamitros M, Kyriakou I, Maigne L, Meylan S, Murakami K, Okada S, Payno H, Perrot Y, Petrovic I, Pham QT, Ristic-Fira A, Sasaki T, Štěpán V, Tran HN, Villagrasa C, Incerti S 2015 Track structure modeling in liquid water: A review of the Geant4-DNA very low energy extension of the Geant4 Monte Carlo simulation toolkit, *Phys. Med.* 31(8), 861–874.

Boudaïffa B, Cloutier P, Hunting D, Huels MA, Sanche L 2000 Resonant formation of DNA strand breaks by low-energy (3 to 20 eV) electrons. *Science* 287(5458), 1658–1660.

Buxton GV 1972 Nanosecond pulse radiolysis of aqueous solution containing oproton and hydroxyl radical scavengers. *Proc. R Soc. A* 328, 9–21.

Cobut V, Frongillo Y, Patau JP, Goulet T, Fraser M-J, Gerin J-P 1998 Monte Carlo Simulation of Fast Electron and Proton Tracks in Liquid Water–I. Physical and Physicochemical Aspects. *Radiat.*

Phys. Chem. 51(3), 229–243.

Date H, Sutherland KL, Hasegawa H, Shimozuma M 2007 Ionization and excitation collision processes of electrons in liquid water. *Nucl. Instr. Meth. B.* 265(2) 515–520.

Draganić ZD, Draganić IG 1975 Formation of primary reducing yields (Geaq- and GH2) in the radiolysis of aqueous solutions of some positive ions. *Int. J. Radiat. Phys. Chem.* 7, 381–386.

Freeman GR 1987 Ionization and charge separation in irradiated materials. In: Freeman, G. R. (ed.) Kinetics of nonhomogeneous processes; Wiley, New York, pp. 19–87.

Friedland W, Dingfelder M, Kundrát P, Jacob P 2011 Track structures, DNA targets and radiation effects in the biophysical Monte Carlo simulation code PARTRAC, *Mutat. Res.* 711(1–2), 28–40.

Fulford J, Nikjoo H, Goodhead DT, O'Neill P 2001 Yields of SSB and DSB induced in DNA by AlK ultrasoft X-rays and a-particles: comparison of experimental and simulated yields. *Int. J. Radiat. Biol.* 77(10), 1053–1066.

Hall EJ, Giaccia AJ 2006 Physics and Chemistry of radiation Absorption, In: Radiobiology for the Radiologist, 7th ed. Lippincott Williams & Wilkins p. 3–11.

Hamm RN, Turner JE, Stabin MG 1998 Monte Carlo simulation of diffusion and reaction in water radiolysis- a study of reactant 'jump through' and jump distances, *Radiat. Environ. Biophys.* 36, 229–234.

Hamill WH 1969 A Model for the Radiolysis of Water. *J. Phys. Chem.* 73, 1311–1347.

Hill MA, Smith FA 1994 Calculation of initial and primary yields in the radiolysis of water, *Radiat. Phys. Chem.* 43, 265–280.

Hirayama H, Namito Y, Bielajew AF, Wilderman SJ, Nelson WR 2005 The EGS5 Code System; Office of Scientific and Technical Information (OSTI), Oak Ridge, TN, USA.

Incerti S, Baldacchino G, Bernal M, Capra, R, Champion C, Francis Z, Guatelli S, Guèye P, Mantero A, Mascialino B, Moretto P, Nieminen P, Rosenfeld A, Villagrasa C Zacharatou C 2010 The Geant4-DNA project. *Int. J. Model. Sim. Sci. Comput.* 01(02), 157–178.

Itikawa Y, Mason N 2005 Cross Sections for Electron Collisions with Water Molecules. *J. Phys. Chem. Ref. Data* 34 (1), 1–22.

Jonah CD, Hart EJ, Matheson MS 1973 Yields and decay of the hydrated electron at times greater than 200 picoseconds. *J. Phys. Chem.* 77, 1838–1843

Jonah CD, Matheson MS, Miller JR, Hart EJ 1976 Yield and decay of the hydrated electron from 100 ps to 3 ns. *J. Phys. Chem.* 80, 1267–1270

Jonah CD, Miller JR 1977 Yield and decay of the OH radical from 200 ps to 3 ns. *J. Phys. Chem.* 81, 1974–1976

Joiner MC, van der Kogel AJ, Steel GG 2009 Introduction: the significance of radiology and radiotherapy for cancer treatment, In: Joiner M, van der Kogel AJ (eds). Basic Clinical Radiobiology. London: Edward Arnold p. 1–10.

Kai T, Yokoya A, Ukai M, Fujii K, Watanabe R 2015a Thermal equilibrium and prehydration processes of electrons injected into liquid water calculated by dynamic Monte Carlo method

Radiat. Phys. Chem. 115 1–5

Kai T, Yokoya A, UkaiMand Watanabe R 2015b Cross sections, stopping powers, and energy loss rates for rotational and phonon excitation processes in liquid water by electron impact, *Radiat. Phys. Chem.* 108, 13–7

Kai T, Toigawa T, Matsuya Y, Hirata Y, Tezuka T, Tsuchida H, Yokoya A 2023 Initial yield of hydrated electron production from water radiolysis based on first-principles calculation, *RSC Adv.* 13, 7076–7086.

Konovalov VV, Raitsimring AM, Tsvetkov YD 1998 Thermalization lengths of "subexcitation electrons" in water determined by photoinjection from metals into electrolyte solutions, *Radiat. Phys. Chem.* 32, 623–632.

Kreipl MS, Friedland W, Paretzke HG 2009 Time- and space-resolved Monte Carlo study of water radiolysis for photon, electron and ion irradiation. *Radiat. Environ. Biophys.* 48, 11–20.

Lampe N, Karamitros M, Breton V, Brown JMC, Sakata D, Sarramia D, Incerti S 2018 Mechanistic DNA damage simulations in Geant4-DNA Part 2: Electron and proton damage in a bacterial cell. *Phys. Med.* 48, 146–155.

LaVerne JA, Pimblott SM 1991 Scavenger and time dependences of radicals and molecular products in the electron radiolysis of water: examination of experiments and models, *J. Phys. Chem.* 95, 3196–3206.

LaVerne JA 2000 OH radicals and oxidizing products in the gamma radiolysis of water, *Radiat. Res.* 153, 196–200.

Matsuya Y, Kai T, Yoshii Y, Yachi Y, Naijo S, Date H, Sato T 2019 Modeling of yield estimation for DNA strand breaks based on Monte Carlo simulations of electron track structure in liquid water, *J. Appl. Phys.* 126, 124701.

Matsuya Y, Nakano T, Kai T, Shikazono N, Akamatsu K, Yoshii Y, Sato T 2020 A Simplified Cluster Analysis of Electron Track Structure for Estimating Complex DNA Damage Yields. *Int. J. Mol. Sci.* 21, 1701.

Matsuya Y, Kai T, Sato T, Liamsuwan T, Sasaki K, Nikjoo H 2021 Verification of KURBUC-based ion track structure mode for proton and carbon ions in the PHITS code, *Phys. Med. Biol.* 66, 06NT02.

Matsuya Y, Kai T, Sato T, Ogawa T, Hirata Y, Yoshii Y, Parisi A, Liamsuwan T 2022 Track-structure modes in particle and heavy ion transport code system (PHITS): application to radiobiological research. *Int. J. Radiat. Biol*. 98(2), 148–157.

Muroya Y, Lin M, Wu G, Iijima H, Yoshii K, Ueda T, Kudo H, Katsumura Y 2005 A re-evaluation of the initial yield of the hydrated electron in the picosecond time range. *Radiat. Phys. Chem.* 72, 169–172.

Peak JG, Ito T, Robb FT, Peak MJ 1995 DNA Damage Produced by Exposure of Supercoiled Plasmid DNA to High- and Low-LET Ionizing Radiation: Effects of Hydroxyl Radical Quenchers, *Int. J. Radiat. Biol.* 67(1), 1–6.

Pastina B, LaVerne JA 1999 Hydrogen Peroxide Production in the Radiolysis of Water with Heavy

Ions. *J. Phys. Chem. A* 103(11), 1592–1597.
Pimblott SM, LaVerne JA 1997 Stochastic simulation of the electron radiolysis of water and aqueous solutions. *J. Phys. Chem. A* 101, 5828–5838.
Plante I, Cucinotta FA 2008 Ionization and excitation cross sections for the interaction of HZE particles in liquid water and application to Monte-Carlo simulation of radiation tracks. *New J. Phys.* 10, 1–15.
Plante I, Devroye L 2017 Considerations for the independent reaction times and step-by-step methods for radiation chemistry simulations. *Radiat. Phys. Chem.* 139, 157–172.
Plante I 2021 A review of simulation codes and approaches for radiation chemistry. *Phys. med. Biol.* 66 03TR02.
Sato T, Iwamoto Y, Hashimoto S, Ogawa T, Furuta T, Abe S Kai T, Tsai P-E, Matsuda N, Iwase H, Shigyo N, Sihver L, Niita K 2018 Features of Particle and Heavy Ion Transport code System (PHITS) version 3.02. *J. Nucl. Sci. Technol*. 55(5–6), 684–690.
Shin W-G, Ramos-Mendez J, Faddegon B, Tran HN, Villagrasa C, Perrot Y, Okada S, Karamitros M, Emfietzoglou D, Kyriakou I, Bordage MC, Sakata D, Guatelli S, Choi HJ, Min CH, Lee SB, Incerti S 2019 Evaluation of the influence of physical and chemical parameters on water radiolysis simulations under MeV electron irradiation using Geant4-DNA. *J. Appl. Phys.* 126 (11), 114301.
Shin W-G, Ramos-Mendez J, Tran NH, Okada S, Perrot Y, Villagrasa C, Incerti S 2021 Geant4-DNA simulation of the pre-chemical stage of water radiolysis and its impact on initial radiochemical yields. *Phys. Med.* 88, 86–90.
Shiina T, Watanabe R, Shiraishi I, Suzuki M, Sugaya Y, Fujii K, Yokoya A 2013 Induction of DNA damage, including abasic sites, in plasmid DNA by carbon ion and X-ray irradiation, *Radiat. Environ. Biophys.* 52, 99–112.
Sumiyoshi T, Katayama M 1982 The yield of hydrated electrons at 30 picoseconds. Chem. Lett. 11, 1887–1890.
Terrissol M, Beaudre A 1990 Simulation of space and time evolution of radiolytic species induced by electrons in water, *Radiat. Prot. Dosim.* 31, 175–177.
Tomita H, Kai M, Kusuma T, Ito A 1997 Monte Carlo simulation of physicochemical processes of liquid water radiolysis. *Radiat. Environ. Biophys*. 36, 16–22.
Tomita H, Kai M, Kusama T, Ito A 1998 Monte Carlo simulation of DNA strand-break induction in supercoiled plasmid pBR322 DNA from indirect effects, *Radiat. Environ. Biophys.* 36, 235–241.
Turner JE, Hamm RN, Wright HA, Ritchie RH, Magee JL, Chatterjee A, Bolch WE 1988 Studies to link the basic radiation physics and chemistry of liquid water, *Radiat. Phys. Chem.* 32, 503–510.
Uehara S 1986 The development of a Monte Carlo code simulating electron–photon showers and its evaluation by various transport benchmarks. *Nucl. Instrum. Methods B.* 14, 559–570.
Uehara S, Nikjoo H 2006 Time- and space-resolved Monte Carlo study of water radiolysis for photon,

electron and ion irradiation. *Radiat. Environ. Biophys.* 48, 11–20.

Wang F, Schmidhammer U, Larbre JP, Zong Z, Marignier JL, Mostafavi M 2018 Time-dependent yield of the hydrated electron and the hydroxyl radical in D2O: a picosecond pulse radiolysis study. *Phys. Chem. Chem. Phys*. 20, 15671.

Watanabe R, Saito K 2001 Monte Carlo simulation of water radiolysis in oxygenated condition for monoenergetic electrons from 100 eV to 1MeV, *Radiat. Phys. Chem.* 62, 217–228.

Wang CR, Nguyen J, Lu QB 2009 Bond breaks of nucleotides by dissociative electron transfer of nonequilibrium prehydrated electrons: a new molecular mechanism for reductive DNA damage. *J. Am. Chem. Soc.* 131(32), 11320–2.

Wolff RK, Bronskill MJ, Aldrich JE, Hunt JW 1973 Picosecond pulse radiolysis. IV. Yield of the solvated electron at 30 picoseconds. *J Phys. Chem.* 77, 1350–1355.